ASME 2016 International Design Engineering Technical Conferences and Computers and Information in Engineering Conference
IDETC 2016
August 21-24, 2016, Charlotte, North Carolina

IDETC2016-60291

DNA-STRUCTURED LINEAR ACTUATORS

Kyle Zampaglione
Tesla Motors, Inc.
Tesla Factory 45500 Fremont Blvd
Fremont, California 94538
kzampaglione@teslamotors.com

Andrew P. Sabelhaus*
Lee-Huang Chen
Alice M. Agogino
Berkeley Emergent Space
Tensegrities (BEST) Lab
Department of Mechanical Engineering
University of California Berkeley
Berkeley, California 94705
apsabelhaus*, leehuanc, agogino @berkeley.edu

Adrian K. Agogino
University Affiliated Research Center,
University of California Santa Cruz
Robust Software Engineering Group,
NASA Ames Research Center
Moffet Field, California 94035
adrian.k.agogino@nasa.gov

ABSTRACT

This work presents a series of DNA-structured linear actuators that have high displacements and compact profiles. These actuators operate by twisting and untwisting a double helix that resembles a DNA molecule. Unlike most similarly-motivated twisted string actuators (TSAs), these DNA-structured actuators can have the ability to exert both push and pull forces on a load. Thus, although originally designed for cable-driven robotics, these actuators have the ability to work as part of many different mechatronic systems. Two inherently different actuator designs were investigated, one with straight-line edges (rails) and one with helical rails. Two mathematical models of angular rotation versus linear displacement were developed and simulated, one for each design, and three prototypes were constructed to validate the models. The final prototype was tested for displacement, restorative torque, and pull force characteristics. This last prototype showed a 30.5 cm stroke for a 40.5 cm actuator, or a displacement of 75.3% of its total length.

INTRODUCTION

Modern robotic systems often need compact linear actuators that have large displacements. In particular, mobile robots that are actuated by cables must house their mechanisms within their structure, and are subject to many design constraints related to volume and desired actuator performance. One example of such design-constrained cable-driven robots are tensegrity systems, which move by changing the lengths of the cables which hold their structures together [1, 2]. These robots, like others, require actuators to fit into small spaces while providing relatively long stroke lengths (displacements) for moving their cables.

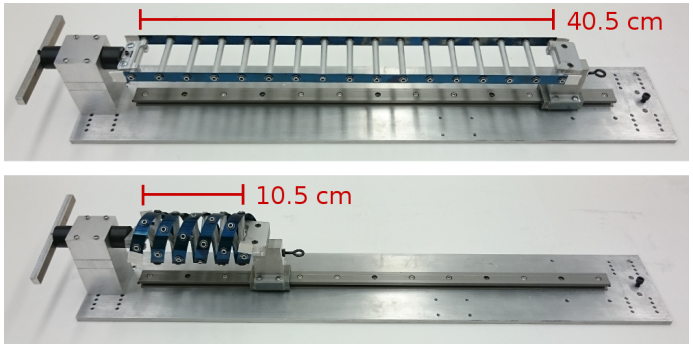

FIGURE 1: PROTOTYPE OF A DNA-STRUCTURED LINEAR ACTUATOR WITH METAL RAILS. TOP: EXTENDED. BOTTOM: RETRACTED.

The DNA-structured linear actuators in this work seek to provide such a design. Like the related concept of twisted-string actuation (TSA), these actuators shorten their lengths by twisting materials around each other, making efficient use of their space. However, unlike many TSAs which have at most practical displacements of roughly 30% of their maximum length [3], these DNA-structured actuators have exhibited displacements up to 75.3% of their lengths. These designs also have the ability to exert both push and pull forces on their load, preventing the need for multiple juxtaposed actuators as in past work [4].

Following a review of past work, two different actuator design paradigms are presented. Analytical models are created for linear displacement versus input rotation angle, for both types of designs. These models are simulated, and simulation data are discussed. Then, three successive hardware prototypes are introduced. Qualitative testing is performed for all three prototypes, and quantitative tests are performed on the third and final pro-

*Address all correspondence to this author.

totype. These quantitative tests included work on characterizing the actuator's restorative torque as an indicator of the ability to exert push forces. Finally, all these observations are discussed in the context of the practical use of these actuators.

BACKGROUND

Actuators for Cable-Driven Robotics

Untethered cable-driven robots often require actuators with stringent engineering requirements. As opposed to tethered systems, these robots must locate their actuation systems within their structures, requiring actuators to fit into small volumes while still providing large displacements [1,2].

Past work on cable-driven robots often combines the design of the mechanism with the design of the actuation system, which creates some limitations. Mechanisms using cables on spools or reels sacrifice the possibility of designs that exert push forces. These constraints motivate the use of multiple cables attached in opposing directions [5, 6], or in more complex patterns such as those in tensegrity robots [1, 7]. This inability to exert both push and pull forces creates an inherent design challenge for cable-driven systems [8].

Prior Work: Twisted String Actuation

Twisted string actuation (TSA), also called twisted cable actuation or twisted wire actuation, is the use of strings to create length change through twisting. Two or more strings are attached between a rotating element (such as a motor) and a load on which to pull. As the rotation twists the strings, their length is shortened. Extensive work has been performed in designing and characterising these actuators themselves [4, 9–11] as well as in their implementation on physical robots [3,12,13]. Some twisted string actuators separate their strings for longer strokes [13–15].

Past TSA research motivates this DNA-structured actuator work by its efficient use of space constraints. TSAs do not require extra unused room for actuator parts at different points in their stroke, unlike linear actuators with belts [16] or motors attached to lead screws.

However, TSAs have limited ranges of movement, due to either the mechanical failure of the strings themselves [13] or geometric concerns with the maximum possible amount of twist in the cables [15]. A comparison of cable displacements in the literature (see Appendix A) shows most TSAs displacing between 20% and 30% of their total length.

DNA-INSPIRED STRUCTURE

The linear actuators presented in this work are motivated by two similar inspirations from physical structures. First is the rope ladder, where two pieces of rope are separated by stiff rungs. Assuming very flexible rope, the edges of this design would then approximate straight lines. The other inspiration, from the DNA molecule, would be for a design where the rails curve in a helix.

Both physical metaphors have the common property that two flexible rails (strings or strips of material) are separated at a distance by cylindrical rungs. This distance is kept constant by the presence of the rails, unlike prior TSA work.

No prior work was found that used such a structure for actuation. However, similar geometries have been used in patents for past designs for sensing instruments [17] or for passive mechanisms with stiff edges [18].

The work reported in this paper is the topic of a recent master's degree by the first author [19].

ANALYTICAL MODELS

Two different models for these geometries were derived, one for the straight-line rails design and a second for the curved helical rails design. Each of these models describes the relationship between the rotation angle input into the actuator versus the actuator's linear displacement.

Setup and Assumptions

In both of these models, the rungs are W (inches) wide. The total angle of twist of the structure (the input into the actuator) is θ_t (rad). Rungs are assumed to be centered at $(x,y) = (0,0)$ in three-dimensional space, to be fully in the z-plane, and to start with the first rung at height $z = 0$.

Straight-line Rails Actuator Model

The straight-line rails model (Fig. 2) is parameterized by by the angle between two successive rungs, θ, and the length of the rail segment between these rungs, L_i. The z-distance between two rungs is z_i. The outer point of any rung is always at distance $r = W/2$ from the center $(0,0)$. The circle drawn out by a rotating rung consequently has radius r. Onto this circle, a chord can be drawn between the the (x,y) positions of two sequential rungs. This chord, between rungs i and $i+1$, has length c.

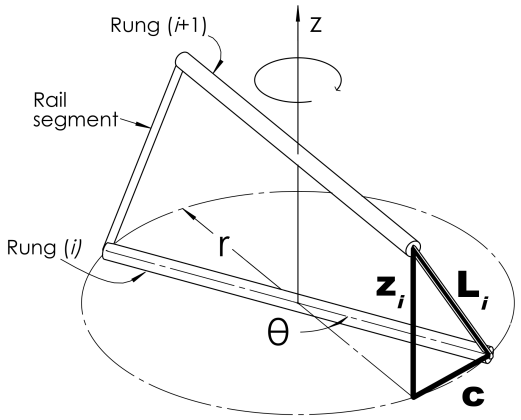

FIGURE 2: MODEL OF THE STRAIGHT-LINE RAILS ACTUATOR. RUNGS ARE SEPARATED BY RAIL SEGMENTS OF LENGTH L_i, AND ARE ROTATED BY θ.

A triangle can be drawn with L_i, z_i, and c, and can be used to calculate z_i as a function of the other two variables.

The chord length c on this base circle (Fig. 3) is a function of angle θ and radius r and can be found using the law of sines:

$$\frac{c}{\sin\theta} = \frac{r}{\sin\beta} = \frac{r}{\sin(\frac{\pi}{2}-\frac{\theta}{2})} = \frac{r}{\cos(\frac{\theta}{2})} \tag{1}$$

$$\therefore \quad c = \frac{r\sin\theta}{\cos(\frac{\theta}{2})} = \frac{2r\sin(\frac{\theta}{2})\cos(\frac{\theta}{2})}{\cos(\frac{\theta}{2})} = 2r\sin\left(\frac{\theta}{2}\right) \tag{2}$$

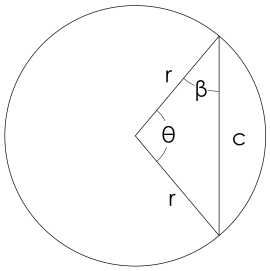

FIGURE 3: THE BASE CIRCLE FOR THE STRAIGHT-LINE RAILS MODEL.

The height z_i can then be found, given θ, r, and L_i.

$$z_i = \sqrt{L_i^2 - c^2} = \sqrt{L_i^2 - \left(2r\sin\left(\frac{\theta}{2}\right)\right)^2} \tag{3}$$

To calculate θ, it is assumed that θ_t will be evenly distributed throughout the rungs, i.e., each rung will twist some amount which will then add to the total rotation. The angle θ will be a fraction of the total θ_t, according to the number of rungs. Since there are $N-1$ spaces between rungs,

$$\theta = \frac{\theta_t}{N-1} \tag{4}$$

The total height of the actuator, z_t can then be found, given the number of rungs and equations (3) and (4).

$$z_t = (N-1)z_i = (N-1)\sqrt{L_i^2 - \left(2r\sin\left(\frac{\theta_t}{2(N-1)}\right)\right)^2} \tag{5}$$

Curved Helical Rails Actuator Model

The equations of a helix are used as the analytical model of the helical-rails actuator (Fig. 4). The rungs are omitted from Fig. 4. The total length of one rail is L_{rail}, and the helix has radius $r = W/2$. The helix curve rises by b inches per radian, so the vertical displacement of the curve is $2\pi b$ per rotation. The curve is thus parameterized by angle θ, where the curve's x, y, and z positions are given by:

$$x = r\cos(\theta), \quad y = r\sin(\theta), \quad z = b\theta \tag{6}$$

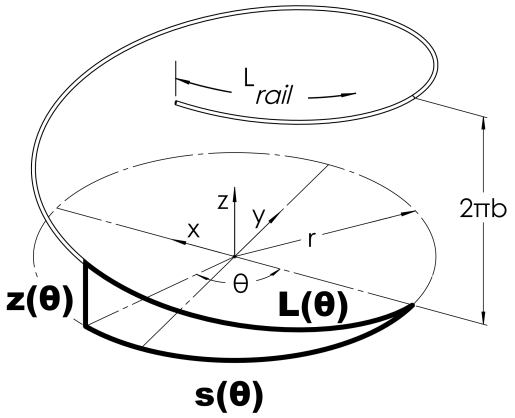

FIGURE 4: MODEL OF THE HELICAL RAILS ACTUATOR. THE HELIX RISES BY $2\pi b$ PER ROTATION.

The rail length $L(\theta)$ can be calculated by noting that the helix forms a triangle on its cylindrical surface between the helix curve itself $L(\theta)$, the helix height $z(\theta)$, and the arc length drawn out on the circular base of the helix's cylinder, $s(\theta)$. Since the radius of the cylinder is r, this arc length on the circular base is $s = r\theta$, thus the rail length is

$$L(\theta)^2 = z(\theta)^2 + s(\theta)^2 = (b\theta)^2 + (r\theta)^2 \tag{7}$$

The constant b can be solved for:

$$L(\theta)^2 = b^2\theta^2 + \left(\frac{W}{2}\right)^2\theta^2 \Rightarrow b = \sqrt{\left(\frac{L(\theta)}{\theta}\right)^2 - \left(\frac{W}{2}\right)^2} \tag{8}$$

Substituting b back in to $z = b\theta$, the total length of the actuator (total height of the helix) can then be calculated from the input angle:

$$z_t = \theta_t\sqrt{\left(\frac{L_{rail}}{\theta_t}\right)^2 - \left(\frac{W}{2}\right)^2} \tag{9}$$

SIMULATIONS

Two different simulations were developed that calculated the actuator displacements, one for each model. All software and data are in MATLAB, and have been made publicly available[1].

For each simulation, the rate of length change of the actuator, $dz/d\theta$, was also calculated. Qualitatively, these rate of length change plots give information about the amount of force that the actuators can exert on a load. If input torque is kept constant, and input rate of rotation is kept constant, then output force will vary in relationship to $dz/d\theta$. An analytical expression of this relationship is left for future work.

[1] https://github.com/BerkeleyExpertSystemTechnologiesLab/dna-actuators

Straight-Line Rails Actuator Simulation

For the straight-line rails actuator model, maximum displacement for an actuator would occur when the rung width W and rung spacing L_i were equal. Then, with a rotation of π between two successive rungs, the length between them would be zero. Thus, in the simulations, the rung width and spacing were kept at a 1:1 ratio, $W = L_i$. All distances are in inches.

Fig. 5 shows a visualization of the structure with $N = 10$ rungs in simulation, where $W = L_i = 1$ inch. These dimensions were chosen to obtain an intuitive understanding of how a reasonably-sized prototype might behave.

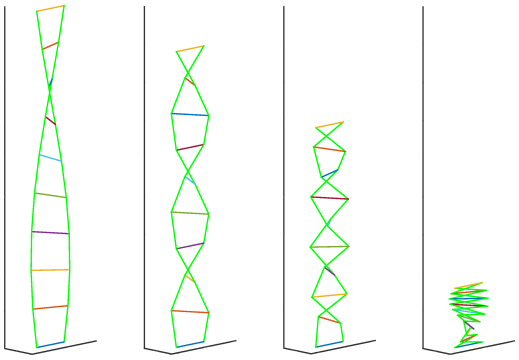

FIGURE 5: STRAIGHT-LINE RAILS MODEL SIMULATION FOR VARYING INPUT ANGLES. LEFT TO RIGHT: $\pi, 3\pi, 5\pi, 8\pi$ RADIANS.

Fig. 6 shows displacements for different size actuators. Each model used $N = 10$ rungs. The rung spacing/width was varied together, such that the actuators were scaled versions of each other. The figure shows that, although the different size actuators have different lengths throughout their stroke, each of them reaches (theoretically) zero length after the same set number of input rotations. This zero length location is at 9π rad, which is $(N-1)\times\pi$ for this $N = 10$ rung model.

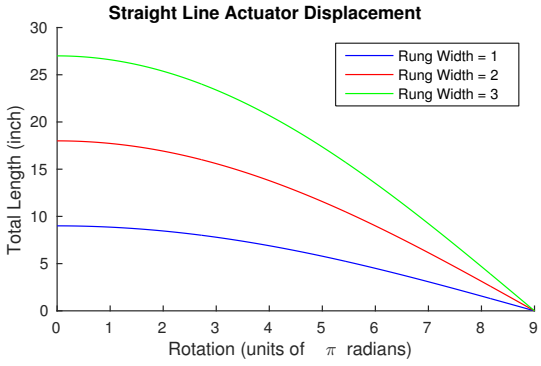

FIGURE 6: DISPLACEMENT SIMULATION FOR THREE STRAIGHT-LINE ACTUATOR SIZES.

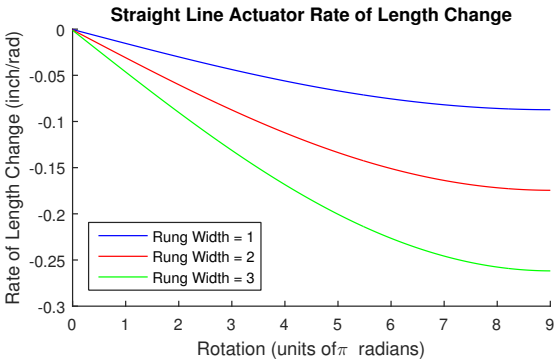

FIGURE 7: RATE-OF-LENGTH-CHANGE SIMULATION FOR THREE STRAIGHT-LINE ACTUATOR SIZES.

The rate of change of the length of the actuator is shown for these tests in Fig. 7, using the same $N = 10$ rung structure. All plots increase in (negative) rate of change throughout their stroke. This implies that the actuator can apply less and less force on a load throughout its stroke. This qualitative observation demonstrates a tradeoff in practical applications of this actuator: though it has a large displacement, there will only be some range of this displacement where it can apply useful amounts of force.

Curved Helical Rails Actuator Simulation

The height of the helical rail model is independent of the number of rungs, as shown in equation 9. The rungs here only serve to keep the two helices separated by a distance. This simulation only depends on the rung width (radius of the helix $W/2$), total rail length L_{rail}, and input twist angle θ_t.

Fig. 8 shows a visualization of the structure with $L_{rail} = 10$ (in.) and $W = 2$ (in.) in simulation, again chosen to give an intuitive sense of the behavior of a reasonably-sized prototype.

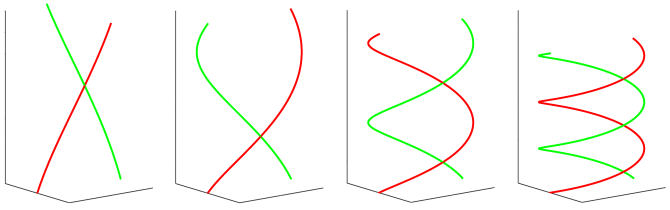

FIGURE 8: HELICAL RAILS MODEL SIMULATION FOR VARYING INPUT ANGLES. LEFT TO RIGHT: $\frac{\pi}{2}, \pi, 2\pi, 3\pi$ RADIANS.

Unlike the straight-line rail model, the number of rotations to full compression varies with the length of the actuator. Fig. 9 shows the displacement for an actuator with $L_{rail} = 10$ and four different rung widths. The equations of motion break down numerically past approximately 3 units in length, so all data are reported only until that point.

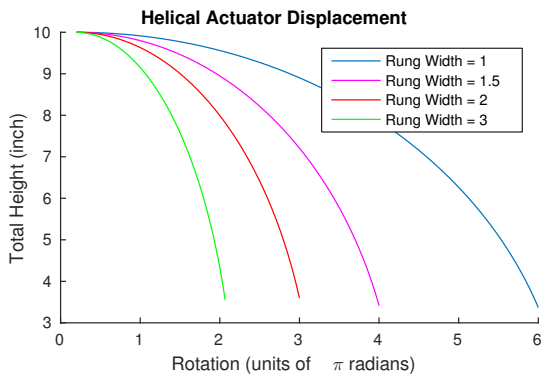

FIGURE 9: DISPLACEMENT SIMULATION FOR FOUR HELICAL ACTUATOR SIZES.

The rate of change of the length of the helical rails actuator is shown for these tests in Fig. 10. These show a more extreme drop in $dz/d\theta$ in comparison to the straight-line model, which demonstrates a more extreme tradeoff in the actuator's ability to apply force on a load throughout its stroke. This observation has design implications relating to the choice of motor to rotate the actuator.

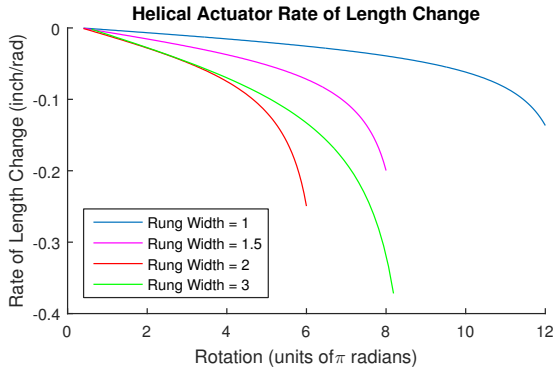

FIGURE 10: RATE-OF-LENGTH-CHANGE SIMULATION FOR FOUR HELICAL ACTUATOR SIZES.

PROTOTYPE DESIGNS AND QUALITATIVE TESTING

Three prototypes were constructed for testing. The first prototype was designed to match the straight-line rails model, with wire rope as its rails. The second and third prototypes were constructed to match the curved helical rails model, with thin strips of material as their rails. Qualitative testing was performed on all three prototypes, and quantitative tests were performed on the third.

Straight-line Rail Prototype Design and Assembly

The straight-line rail prototype used 0.119 cm (3/64 inch) diameter 18-8 stainless steel wire rope with a 7x19 grouping as the rail material, and 5.08 cm long by 0.64 cm diameter (2" by 1/4") 6061 aluminum rods as the rungs. Holes were drilled through the

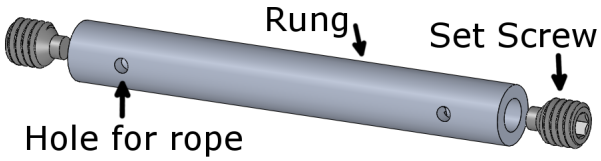

FIGURE 11: EXPLODED VIEW OF A SINGLE RUNG OF THE STRAIGHT-LINE RAIL PROTOTYPE.

cylindrical face of the rungs to pass the wire rope through, and the flat faces of the rungs were tapped for 10-32 soft point set screws to constrain the rope. Fig. 11 shows an exploded view of the rung assembly.

Constructing this actuator consisted of sliding rungs onto two wire ropes. In order to position the rungs consistently on the cables, a rig was created that held the rungs in place during assembly, at a set spacing of 3.81 cm (1.5") between rails.

This prototype has one distinct difference from the model. In the model, the straight-line rails attach to the rungs at an angle that changes throughout motion. However, in the prototype, the rope rails are constrained and cannot rotate with respect to the rungs. Consequently, the angle change must happen as a bend in the rope itself, and the prototype will not have straight-line rails but instead slightly curved rope rails. This was initially taken as a reasonable rapid prototyping design tradeoff.

Straight-line Rail Prototype Testing

The straight-line rail prototype was qualitatively tested through twisting by hand. This testing showed significant differences between the analytical model and the prototype, motivating the move to the latter two designs.

After approximately 3π rotations (540 degrees) for a 7-rung model, held in tension, the ropes would snap together between the rungs, and the rungs would contact each other. This indicates a bifurcation in the underlying mechanics model. Though the analytical model did not show the straight-line rails ever coming into contact, this prototype was unstable under tension. Fig. 12 shows this model just before the snap occurs (left), and then just after (right).

This behavior was initially attributed to imperfect assembly. Although the assembly rig tried to create equal spacing between each set of rungs, irregularity in tension during assembly would cause small spacing variations. However, even with more precisely-spaced rungs, the bifurcation still occurs. The right side image in Fig. 13 shows three rungs where the ropes simply cross over each other, but which is still unlike the simulation.

Since the ropes on the right-side image in Fig. 13 show noticeable bending, it is possible that the rotational constraint on the design causes these issues. Though there are potential remedies to this design that still used rope rails, these remedies were simpler to implement when using flat strips of material instead.

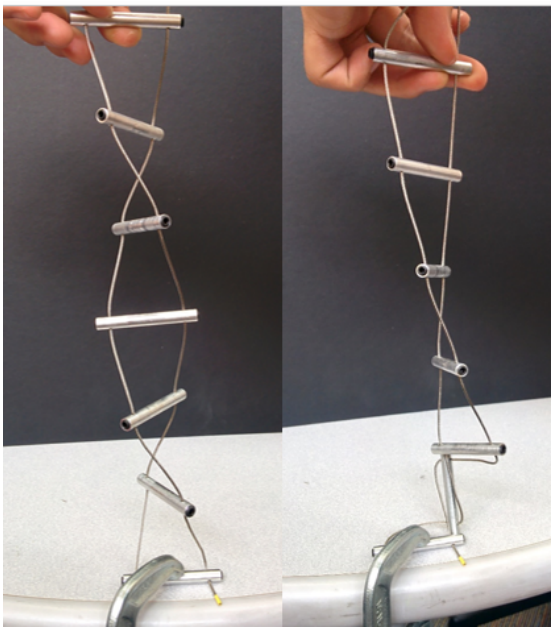

FIGURE 12: LEFT: STRAIGHT-LINE RAIL PROTOTYPE WITH WIRE ROPE RAILS AND 7 RUNGS, JUST BEFORE SNAPPING BIFURCATION OCCURS. RIGHT: JUST AFTER THE SNAP.

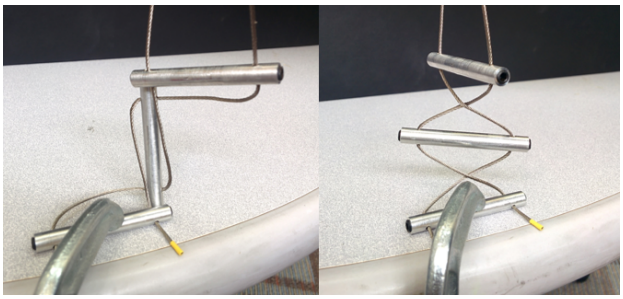

FIGURE 13: LEFT: SNAPPING BIFURCATION WITH UNEVENLY-SPACED RAILS. RIGHT: SNAPPING BIFURCATION WITH PRECISE AND EVEN SPACING.

Curved Helical Rail Prototype 1: Nylon, Design

The second prototype, constructed with a thin nylon strip as the rail, was designed to account for the problems seen in the first prototype. Specifically, the rungs were allowed to rotate freely. Fig. 14 shows an image of this prototype in three different states: flat, partially twisted, and fully twisted.

This structure consisted of two long, thin strips of nylon connected together by aluminum rungs. The nylon rails were 1.27 cm high by 0.079 cm thick (1/2" by 0.031"). With a 2.54 cm (1") spacing between rungs and 15 rungs, each rail was just over 38.1 cm (15") long. The rails were laser-cut from nylon sheet material. The rungs were again made from 5.08 cm long by 0.64 cm diameter (2" by 1/4") 6061 aluminum rods. However, the rungs

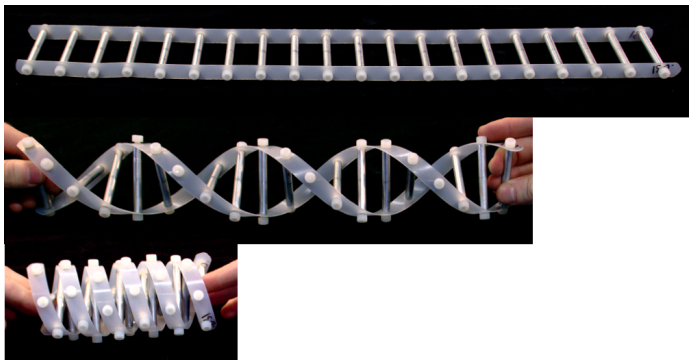

FIGURE 14: CURVED HELICAL RAILS PROTOTYPE 1: NYLON RAILS. TOP: UNTWISTED. MIDDLE: PARTIALLY TWISTED. BOTTOM: FULLY TWISTED.

were tapped on each end for a 10-32 screw fastener. The prototype was assembled by inserting fasteners through the nylon sheet and screwing them into the rails. Then, after all the rungs were secured, each fastener was rotated 1/8 of a turn in reverse to allow the rungs to rotate freely.

Curved Helical Rail Prototype 1: Nylon, Testing

This prototype behaved qualitatively like the curved helical rails model when twisted by hand. Under small-to-medium loads, it did not collapse, unlike the rope prototype.

Two desired design changes were identified in this model. First, the nylon rails were the weakest component in the actuator, and were observed to fail under moderate loading by hand. A stiffer material was desired so that higher loads could be applied. Second, although the rails were allowed to rotate at their attachment point to the rungs, they were still compressed flat in that section. This phenomenon, shown by the red arrows in Fig. 15, leads to an uneven helical curvature of the rails. A new design was desired that allowed for the rails to curve more naturally so as to both fit the model better and to prevent unnecessary stress concentrations.

Curved Helical Rail Prototype 2: Spring Steel, Design

The third prototype, shown in Fig. 16, had spring steel strips in place of the nylon strips in the second prototype. The rails for this model were made from 1.27 cm high by 0.018 cm thick (1/2" by 0.007") 1095 blue-tempered spring steel, cut by a water jet in the same way the nylon was cut with a laser cutter. Like the nylon prototype, a 2.54 cm (1") spacing between the rungs was used in an attempt to reinforce against deformation in the rails. The rungs were again made from 5.08 cm long by 0.64 cm diameter (2" by 1/4") 6061 aluminum rods.

In order to create the desired room for the steel sheets to curve around the rod end (unlike the nylon flattening phenomenon), a small wave spring assembly was designed for the ends of the rods. A step in the shaft of 0.43 cm length, reducing

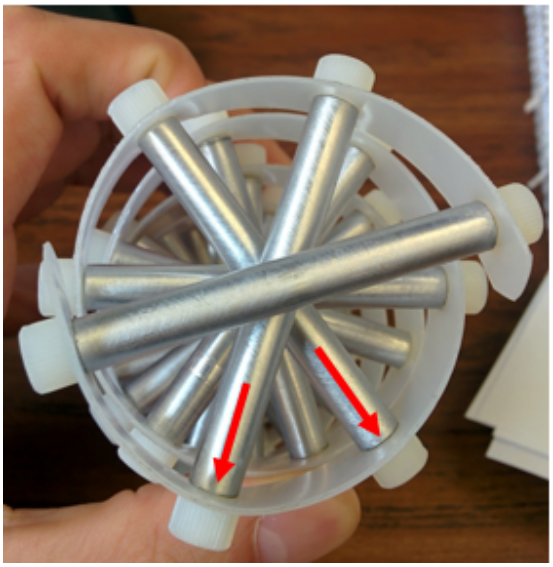

FIGURE 15: NYLON RAILS, PRESSED FLAT AT THE CONNECTION POINT WITH THE RUNGS.

FIGURE 16: CURVED HELICAL RAILS PROTOTYPE 2: SPRING STEEL RAILS.

it to a diameter of 0.48 cm (3/16”), was machined onto either end of the rung, and a groove for a snap ring is machined toward the end of the step. The rail, spacing shims, wave spring, and snap ring are attached onto that end. Fig. 17 shows an exploded view of this design.

Curved Helical Rail Prototype 2: Spring Steel, (Qualitative) Testing

The wave spring assembly allowed for the tuning of the spring forces on the steel rails at the end of the rungs. Fig. 18 shows the prototype, held vertically, with two different levels of preloading. The top image shows the assembly with only 0.051 cm (0.002”) of shims at the rungs, which allowed for too much play in the design, as shown by the structure sagging against gravity. The bottom image shows the assembly as used for testing, with extra shims, for 0.127 cm (0.005”) of displacement against the wave springs.

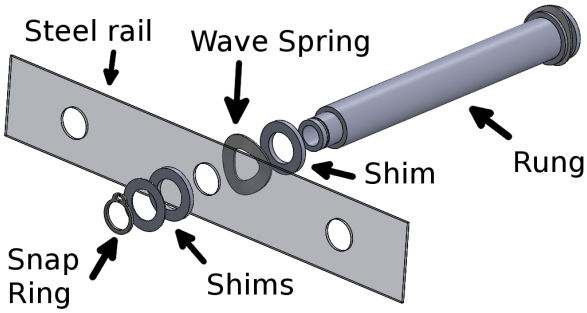

FIGURE 17: RUNG ASSEMBLY FOR THE STEEL RAILS PROTOTYPE.

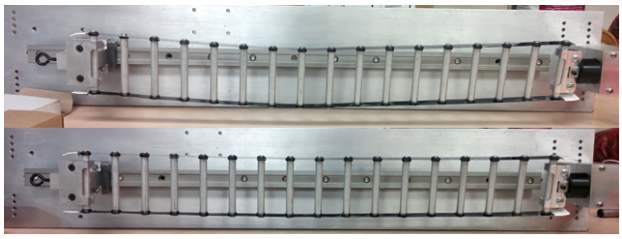

FIGURE 18: THE STEEL RAIL PROTOTYPE WITH INSUFFICIENT PRELOADING (TOP) AND WITH HIGHER PRELOAD (BOTTOM).

Additionally, the steel rail prototype resisted twisting, and would untwist back to a flat position when released. This phenomenon was not observed in the rope rail prototype, and was weakly observed in the nylon prototype. Investigating the extent of this restorative torque within the actuator itself, under no loading, would allow for design guidelines about using the actuator in both push and pull.

QUANTITATIVE PROTOTYPE TESTING

Three types of tests were performed on the spring steel rails actuator prototype. Tests of input rotation versus linear displacement were motivated by a desired comparison with the analytical models. Based on the observation that the prototype has some inherent stiffness, tests were performed to determine its restorative torque under no loading. Finally, pull tests were performed to determine the displacements at which the actuator would fail or deform for different loads.

Test Fixture

One primary test fixture was used. This fixture, repeated here in Fig. 19, suspends the prototype between a hand-turned handle and a moving mount on a carriage. The carriage mount provides the necessary opposing torque to allow the actuator to twist, while also allowing the free end to move. The tested prototype had $N = 17$ rungs.

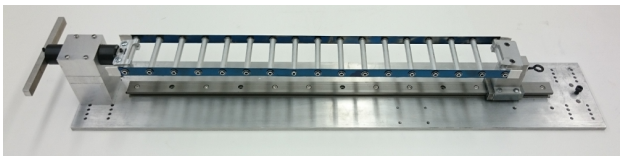

FIGURE 19: TEST FIXTURE. THE PROTOTYPE IS SUSPENDED BETWEEN A TURNING HANDLE AND A MOVING MOUNT ON A CARRIAGE.

Each of the tests described below involved manually turning the handle of the test fixture to certain rotation angles. Since these rotations were only determined visually, they are a notable source of error.

Displacement Testing

Using the hand handle on the test fixture, the prototype was turned in 90 degree ($\frac{\pi}{2}$ rad) increments, and its length was measured from the center of the first rung to the center of the last rung, using a metric ruler with 1 mm demarcations. Fig. 20 shows this data plotted alongside simulation data for a helical actuator with the same geometry.

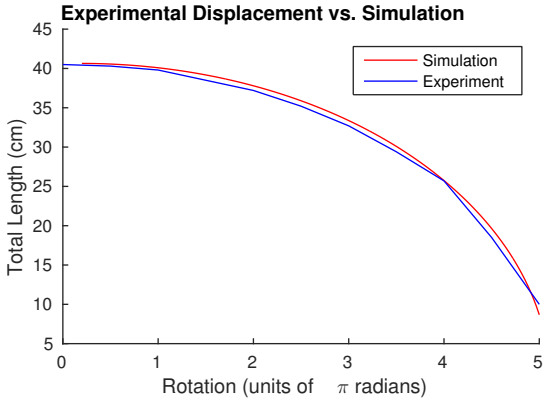

FIGURE 20: DISPLACEMENT EXPERIMENT.

This test was only performed once, so no meaningful statistics are provided here. However, the root mean squared error was calculated between the model and experiment. The error was $RMSE = 0.74$ cm, indicating a particularly accurate model given the noisy data collection procedure.

The minimum and maximum lengths observed in this test were 40.5 cm and 10.0 cm, leading to a total displacement of 75.3% length.

Restorative Torque Testing

For the restorative torque testing, a digital torque meter was attached to the turning handle of the test fixture. No load was attached to the actuator. Measurements in units of pound-inches (lb-in) were taken from the meter at 90 degree ($\frac{\pi}{2}$ rad) rotation increments, which again were hand-twisted and visually identified. This test was performed five times and the results were averaged.

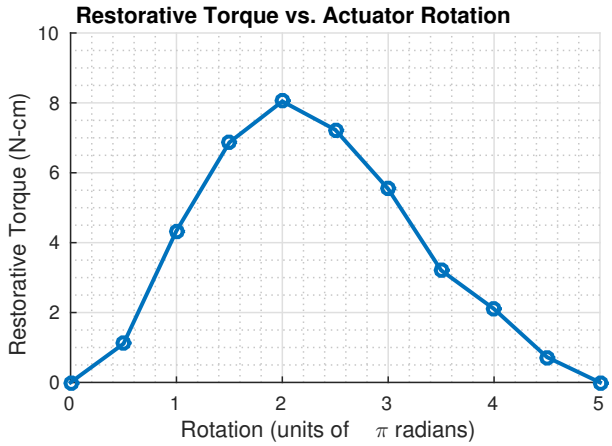

FIGURE 21: RESTORATIVE TORQUE EXPERIMENT, TORQUE VS. ROTATION.

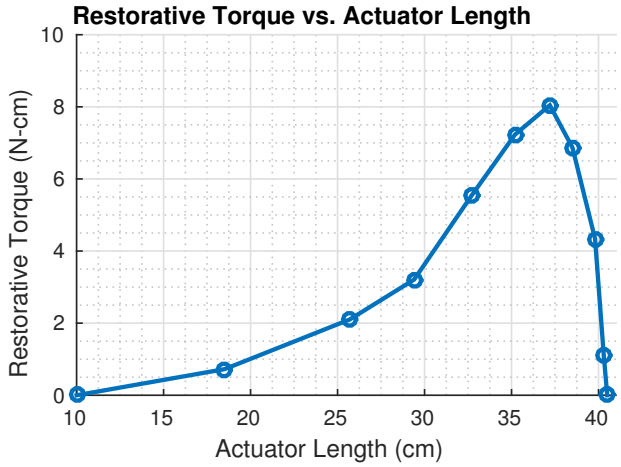

FIGURE 22: RESTORATIVE TORQUE EXPERIMENT, TORQUE VS. LENGTH.

Fig. 21 and 22 show this test, with torque data converted to N-cm and plotted against number of rotations (21) or total actuator length (22). Length data was re-used from the displacement test. The torque peaks at 8.1 N-cm around a 2π rotation angle, at a length of 37.2 cm. This length corresponds to 9% displacement.

Pull Force Testing

Pull force testing was performed to determine rough estimates of how much loading the actuator could withstand. The test fixture for the displacement testing was re-used, and a spring scale was attached to the carriage-mounted free end of the actuator. Fig. 23 shows this setup.

For these tests, the actuator was rotated some specified amount, and then the carriage assembly was pulled back until the actuator began to deform. At the point of deformation, the force

FIGURE 23: TEST FIXTURE FOR THE PULL FORCE EXPERIMENT. A SPRING SCALE IS ATTACHED TO THE LINEAR END OF THE ACTUATOR.

value was read off the spring scale (in N, with 1 N demarcations). Here, deformation is loosely defined to mean the point at which the rails visibly bent out-of-plane, not plastic deformation within the steel. Fig. 24 shows an example of the test procedure.

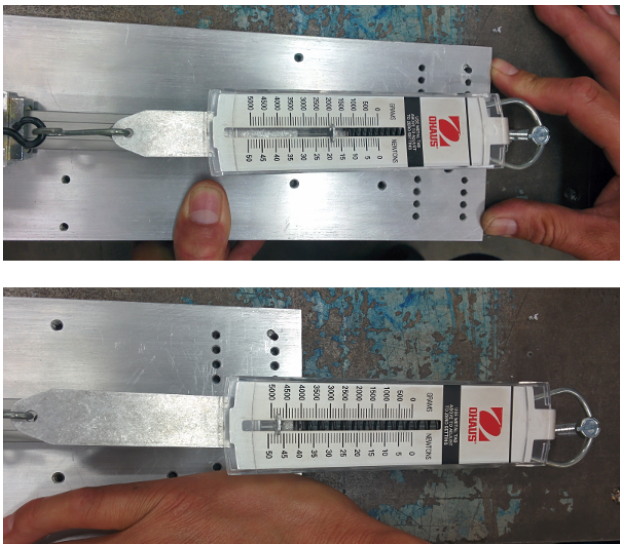

FIGURE 24: PULL FORCE EXPERIMENT EXAMPLE. THE TEST FIXTURE IS PULLED AWAY FROM THE SPRING SCALE ATTACHMENT POINT UNTIL THE ACTUATOR BEGINS TO DEFORM.

This point of deformation was, again, visually determined, thus again, the data presented in this section are notably noisy. Fig. 25 shows these data. Note that no data are provided for the first few rotations of the actuator: the spring scale only read up to 50 N, and all tests less than $5\pi/2$ rotations (450 degrees) exceeded the limits of the scale. Above 4π rotations, the actuator would deform with very little applied force, and test procedures were not accurate enough to record data in that regime.

DISCUSSION

This work provides several notable observations for the design and use of DNA-structured linear actuators, with either straight-line rails or curved double-helix rails. All actuator designs were compact, in that they did not use extra space when actuated, but instead folded into themselves.

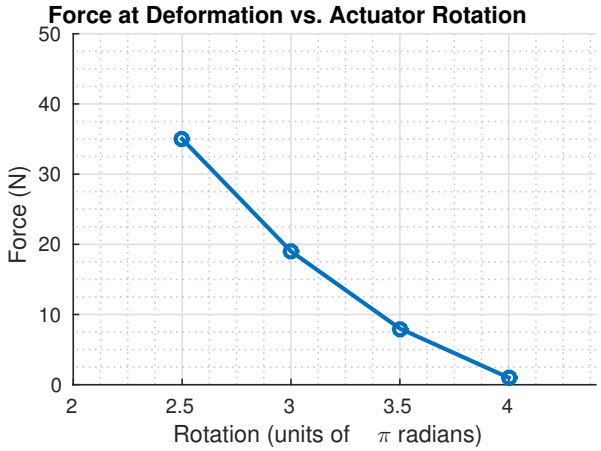

FIGURE 25: PULL FORCE EXPERIMENT.

Designs of these actuators which use straight-line edges suffer from challenges relating to kinematics and instability. The current rope-rail design would not be suitable for practical use. However, design changes are possible that could make this model useful; in particular, incorporating rotating rungs may alleviate many of the problems. The rungs could also be constrained in helical tracks to prevent collapse.

Three observations can be made regarding the mechanical design of the strip material (helical rail) actuators. First, the rungs must be able to rotate with respect to the rails in order for the structure to change shape properly. Second, the rung assembly must allow for the rails to curve naturally around the attachment point; too much pressure flattens the rails. Finally, stiffness is still required at this rail-rung joint to exert some force on the rails; this is needed to reduce play.

The helical displacement model in this work aligns well with experiment, particularly notable given the noisy test procedures.

The data, in general, show these actuators to have large displacements at the potential expense of applied force. The final actuator prototype displaced 75.3% of its length, much more than prior work on twisted cable actuation. However, the rate-of-change data imply that practical use of this actuator would require careful selection of attached components such as motors.

Though no explicit tests of push force were performed to characterize the helical strip rail actuator's full capabilities, the observation of restorative torques and the natural re-extension of the actuator (without loading) show its ability to exert some push force. This torque shows that there is some stiffness within the structure while pushing, and that stiffness could allow a motor to drive the actuator in extension as well as contraction. However, it is unknown how significant these applied extension forces could be before the actuator fails.

FUTURE WORK

More investigation is needed into the development of mechanics models for the helical rails. Future work could involve models of stress for a more theoretical treatment of these designs, including the ability to apply safety factors against plastic deformation.

Such modeling would also benefit from a characterization of actuator performance. Relationships between displacement, stresses, rail geometry, and material properties could be developed. More rigorous mechanical testing would allow for the fitting of parameters to these more useful models.

The rope-rail prototype may be revisited, using rotating rungs, or helical tracks.

Finally, future work may involve practical design considerations of components related to the actuator (motor, actuator housing) for the implementation of these designs in robotics.

ACKNOWLEDGMENT

This work would not have been possible without the help of the many members of the Berkeley Emergent Space Tensegrities Lab at UC Berkeley and the Dynamic Tensegrity Robotics Lab at NASA Ames Research Center's Intelligent Robotics Group. Special thanks in particular to Vytas SunSpiral for his leadership of the team at NASA Ames, and all his effort and feedback for this project.

This work was supported by a NASA Space Technology Research Fellowship, no. NNX15AQ55H. Funding for various parts of this work was provided by NASA ESI Grant No. NNX15AD74G, the NASA Advanced Studies Laboratory at NASA Ames Research Center and UC Santa Cruz, and NSF Graduate Reseach Fellowship no. DGE 1106400.

REFERENCES

[1] Sabelhaus, A. P., Bruce, J., Caluwaerts, K., Manovi, P., Firoozi, R. F., Dobi, S., Agogino, A. M., and SunSpiral, V., 2015. "System design and locomotion of SUPERball, an untethered tensegrity robot". In 2015 IEEE International Conference on Robotics and Automation (ICRA), IEEE, pp. 2867–2873.

[2] Kim, K., Agogino, A. K., Moon, D., Taneja, L., Toghyan, A., Dehghani, B., SunSpiral, V., and Agogino, A. M., 2014. "Rapid prototyping design and control of tensegrity soft robot for locomotion". In 2014 IEEE International Conference on Robotics and Biomimetics (ROBIO), IEEE, pp. 7–14.

[3] Guzek, J. J., Petersen, C., Constantin, S., and Lipson, H., 2012. "Mini Twist: A Study of Long-Range Linear Drive by String Twisting". *Journal of Mechanisms and Robotics,* ***4***(1), feb, p. 014501.

[4] Shoham, M., 2005. "Twisting Wire Actuator". *Journal of Mechanical Design,* ***127***(3), p. 441.

[5] Mao, Y., and Agrawal, S. K., 2012. "Design of a cable-driven arm exoskeleton (CAREX) for neural rehabilitation". *IEEE Transactions on Robotics,* ***28***(4), pp. 922–931.

[6] Yuan, J., Wan, W., Chen, K., Fang, Q., and Zhang, W., 2014. "Design and Prototyping a Cable-driven Multi-stage Telescopic Arm for Mobile Surveillance Robots". *IEEE International Conference on Robotics and Biomimetics (ROBIO)*, pp. 1845–1850.

[7] Sabelhaus, A. P., Ji, H., Hylton, P., Madaan, Y., Yang, C., Friesen, J., SunSpiral, V., and Agogino, A. M., 2015. "Mechanism Design and Simulation of the ULTRA Spine, a Tensegrity Robot". In ASME International Design Engineering Technical Conference.

[8] Zanotto, D., Rosati, G., and Rossi, A., 2010. "Performance Analysis of Planar Cable-Based Parallel Manipulators". *Proceedings of the ASME 10th Biennial Conference on Engineering Systems Design and Analysis, Vol 3,* ***60***, pp. 789–798.

[9] Palli, G., Natale, C., May, C., Melchiorri, C., and Wurtz, T., 2013. "Modeling and Control of the Twisted String Actuation System". *IEEE/ASME Transactions on Mechatronics,* ***18***(2), apr, pp. 664–673.

[10] Park, I.-W., and SunSpiral, V., 2014. "Impedance controlled twisted string actuators for tensegrity robots". In 14th International Conference on Control, Automation and Systems (ICCAS), IEEE, pp. 1331–1338.

[11] Gaponov, I., Popov, D., and Ryu, J. H., 2014. "Twisted string actuation systems: A study of the mathematical model and a comparison of twisted strings". *IEEE/ASME Transactions on Mechatronics,* ***19***(4), pp. 1331–1342.

[12] May, C., Schmitz, K., Becker, M., and Nienhaus, M., 2013. "Investigation of Twisted String Actuation with a Programmable Mechanical Load Test Stand". In Innovative Small Drives and Micro-Motor Systems, 9. GMM/ETG Symposium, pp. 1–6.

[13] Sonoda, T., and Godler, I., 2010. "Multi-Fingered Robotic Hand Employing Strings Transmission Named Twist Drive ". *IEEE/RSJ International Conference on Intelligent Robots and Systems (IROS)*, pp. 2527–2528.

[14] Godler, I., Hashiguchi, K., and Sonoda, T., 2010. "Robotic finger with coupled joints: A prototype and its inverse kinematics". In 2010 11th IEEE International Workshop on Advanced Motion Control (AMC), IEEE, pp. 337–342.

[15] Singh, H., Popov, D., Gaponov, I., and Ryu, J.-H., 2015. "Passively adjustable gear based on twisted string actuator: Concept, model and evaluation". *Robotics and Automation (ICRA), 2015 IEEE International Conference on*, pp. 238–243.

[16] Joël Bourc'His, 2007. "Linear belt actuator". *US Patent US7270619 B2*.

[17] Brady, J. M., 1951. "Pressure measuring device". *US Patent US2564669 A*.

[18] Lemaire, R. A., 1999. "Frame collapsible and extendable by means of a turning movement". *US Patent US5941400 A*.

[19] Zampaglione, K., 2015. "DNA-Structured Linear Actuator for Tensegrity Robots". Master's report, University of California Berkeley.

Appendix A: Calculation of Twisted String Actuator Displacements from Related Work

Actuator displacement data for related work are cited throughout this paper. We refer to displacement percentage as $\%D = (L_0 - L_f)/L_0$, where L_0 and L_f are the initial and final actuator lengths, respectively.

In table 1, all lengths are assumed to be experimentally measured. An asterisk (*) denotes that the cited work is unclear, and the numbers may only be from theory. The number of significant figures are from the cited work.

TABLE 1: Twisted Cable Actuator Performance in Related Work.

Reference	L_0, cm	L_f, cm	$\%D$	Source? *
Godler '10	2.5	1.0	**40%**	Fig. 4 *
Sonoda '10	2.5	1.0	**40%**	Fig. 3 *
Palli '13	5.000	3.310	**34%**	Fig. 1 *
Guzek '12	41	28	**32%**	Fig. 5b
Suzuki '05	10	2.5	**25%**	Fig. 4
Park '14	16.9	3.9	**23%**	Fig. 4
Gaponov '14	-	-	**18%**	Fig. 11
Singh '15	33.3	6.0	**18%**	Fig. 6
Palli '13	2	0.28	**14%**	Fig. 7
Shoham '05	1.0	0.04	**4%**	Fig. 7